

Retrieval of Ocean Surface Wind Speed and Wind Direction Using Reflected GPS Signals

ATTILA KOMJATHY, MICHAEL ARMATYS, DALLAS MASTERS, AND PENINA AXELRAD

CCAR, University of Colorado, Boulder, Colorado

VALERY ZAVOROTNY

NOAA/Environmental Technology Laboratory, Boulder, Colorado

STEVEN KATZBERG

NASA Langley Research Center, Hampton, Virginia

(Manuscript received 23 September 2002, in final form 3 August 2003)

ABSTRACT

Global positioning system (GPS) signals reflected from the ocean surface can be used for various remote sensing purposes. Some possibilities include measurements of surface roughness characteristics from which the rms of wave slopes, wind speed, and direction could be determined. In this paper, reflected GPS measurements that were collected using aircraft with a delay mapping GPS receiver are used to explore the possibility of determining ocean surface wind speed and direction during flights to Hurricanes Michael and Keith in October 2000. To interpret the GPS data, a theoretical model is used to describe the correlation power of the reflected GPS signals for different time delays as a function of geometrical and sea-roughness parameters. The model employs a simple relationship between surface-slope statistics and both a wind vector and wave age or fetch. Therefore, for situations when this relationship holds there is a possibility of indirectly measuring the wind speed and the wind direction. Wind direction estimates are based on a multiple-satellite nonlinear least squares solution. The estimated wind speed using surface-reflected GPS data collected at wind speeds between 5 and 10 m s⁻¹ shows an overall agreement of better than 2 m s⁻¹ with data obtained from nearby buoy data and independent wind speed measurements derived from TOPEX/Poseidon, European Remote Sensing (ERS), and QuikSCAT observations. GPS wind retrievals for strong winds in the close vicinity to and inside the hurricane are significantly less accurate. Wind direction agreement with QuikSCAT measurements appears to be at the 30° level when the airplane has both a stable flight level and a stable flight direction. Discrepancies between GPS retrieved wind speeds/directions and those obtained by other means are discussed and possible explanations are proposed.

1. Introduction

The use of GPS as a forward-scatter remote sensing tool has become a reality in the last few years (Katzberg and Garrison 1996; Garrison et al. 1997, 1998, 2002; Garrison and Katzberg 2000; Komjathy et al. 1999, 2000; Lin et al. 1999; Armatys et al. 2000). NASA researchers S. J. Katzberg of Langley Research Center (LaRC) and J. L. Garrison, now at Purdue University, have developed a specialized GPS receiver called the Delay-Mapping Receiver (DMR) to measure the reflected signals and have studied the properties of the ocean-reflected signal (Garrison et al. 1997).

Other investigations of ocean-reflected GPS signals are being conducted by the Jet Propulsion Laboratory (JPL) and the European Space Agency (ESA), and are focused primarily on the application of reflected GPS signal tracking to altimetry proposed by Martin-Neira (1993). These groups have conducted a number of experiments from static locations and aircraft, and have investigated signals received from a spaceborne antenna (Treuhaft et al. 2001; Lowe et al. 2000, 2002; Martin-Neira et al. 2001).

Using the DMR and models to predict the interaction of the L1 GPS signal at 1575.42 MHz, researchers at NASA Langley Research Center, Purdue University, and the University of Colorado at Boulder have been able to estimate speed of steady winds on the ocean surface with an accuracy of about 2 m s⁻¹ for moderate wind speeds. Results to date have advanced the understanding of reflected GPS signals and provide direct experimental

Corresponding author address: Attila Komjathy, California Institute of Technology, Jet Propulsion Laboratory, MS 238-634A, 4800 Oak Grove Dr., Pasadena, CA 91109.
E-mail: Attila.Komjathy@jpl.nasa.gov

evidence of their application to ocean remote sensing and mapping.

The GPS bistatic scattering model employed in this paper's estimation process was developed by Zavorotny and Voronovich (2000) (see also Komjathy et al. 2000). The scattering model employs a bistatic radar equation with the geometric optics limit of the Kirchhoff approximation. The sea-roughness spectrum used by the scattering model is that from Elfouhaily et al. (1997). This spectrum and many other available empirical models for the sea-roughness directional spectrum pertain to the case of steady winds far from areas with sharp changes of wind speed and direction such as tropical storms. There are no similar models for hurricanes due to lack of necessary observational data and complexity of air-sea interaction in such objects. Scanning radar altimeter observations show multiple interacting systems of storm-generated surface waves in the interior of hurricanes (Wright et al. 2001).

The scattering model takes the form

$$\begin{aligned} & \langle |Y(\tau, f_c)|^2 \rangle \\ &= T_i^2 \int \frac{|\Re|^2 D^2(\boldsymbol{\rho}) \Lambda^2[\tau - (R_0 + R)/c]}{4\pi R_0^2(\boldsymbol{\rho}) R^2(\boldsymbol{\rho}) q_z^4} \\ & \quad \times |S[f_D(\boldsymbol{\rho}) - f_c]|^2 P\left(-\frac{\mathbf{q}_\perp}{q_z}\right) q^4 d^2\rho, \quad (1) \end{aligned}$$

where $\langle |Y(\tau, f_c)|^2 \rangle$ is the reflected power for any delay bin τ and Doppler offset f_c ; T_i is the integration time in seconds, $\Re(\boldsymbol{\rho}) = \Re[\alpha(\boldsymbol{\rho})]$ is the complex reflectivity of the ocean at L1 being a function of a local incidence angle α with respect to the surface facet at some point $\boldsymbol{\rho}$; D is the antenna gain; Λ is the correlation function of the GPS C/A code; S is the Doppler sync function; P is the probability density function (PDF) of the surface slopes; ρ is the magnitude of the scattering vector \mathbf{q} ; R_0 is the distance from some point on the surface point to the GPS satellite; R is the distance from the GPS receiver to some point on the surface; c is the speed of light; f_D is the Doppler shift at the specular point; f_c is the compensation frequency or the Doppler offset to some point $\boldsymbol{\rho}$; and $\boldsymbol{\rho}$ is a vector from the specular point to some other point on the surface. For our aircraft experiments discussed in this paper, Eq. (1) can be simplified and S set to unity. According to the composite sea surface concept (Valenzuela 1978; Bass and Fuks 1979) used in the scattering model, the surface slopes under the consideration are those created by surface waves with wavenumbers larger than $2\pi \cos\alpha/3\lambda$, where λ is the radio wavelength (Zavorotny and Voronovich 2000).

2. Instrument and data

The use of GPS in a bistatic radar configuration to measure surface properties relies upon our ability to extract information from the reflected signal. For standard GPS navigation applications, the receiver's main

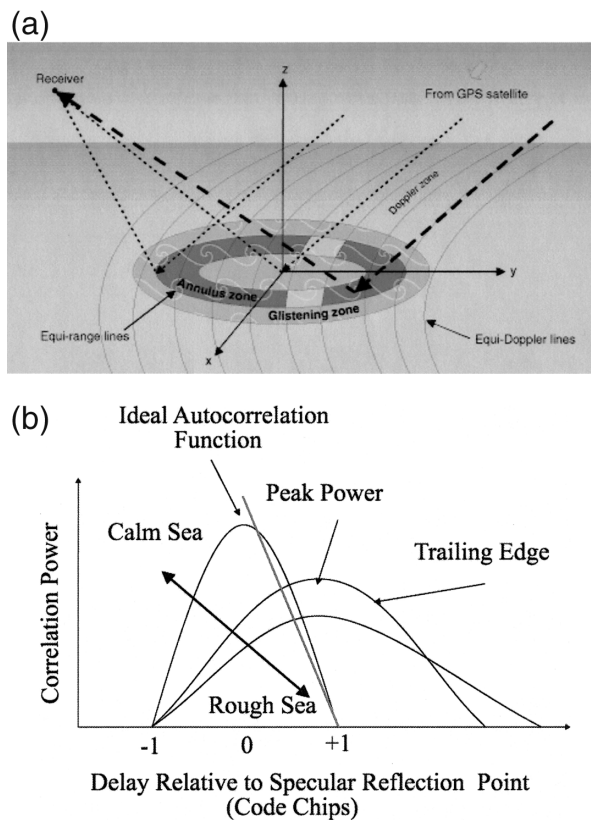


FIG. 1. (a) Illustration for ocean-reflected GPS signals. (b) Correlation function shapes for ideal direct GPS signal and for reflected signals from rough surfaces.

functions are to measure the signal delay from the satellite (the pseudorange measurement) and the rate of change of the range (the Doppler measurement) (see, e.g., Parkinson et al. 1996a,b). Conversely, in our remote sensing application, the primary measurement is the received power from a reflected signal for a variety of delays and Doppler values. The basis of this measurement and its sensitivity to the surface conditions is discussed in the following.

The Delay Mapping Receiver (DMR) is a software configurable General Electric Company (GEC) Plessey (now Mitel Semiconductor) GPS Builder-2 receiver modified to observe reflected left-hand circularly polarized (LHCP) signals from two GPS satellites and to record correlator power at 10 consecutive half-chip intervals. The half-chip intervals are analogous to range bins in a radar receiver and are used to isolate power reflecting from a specific region on the ocean surface called an annulus zone. Signals reflected from the ocean surface originate from a glistening zone (see Fig. 1a) surrounding a nominal specular reflection point. At typical airborne receiver altitudes, incidence angles of forward GPS scatter range as a function of satellite elevation angles between 0° and 70° . The size and shape of the glistening zone are functions of the roughness of the ocean surface. For typical conditions and geometry,

the elliptic glistening zone could be several kilometers by about 10 km in size. To measure the reflected power from this glistening zone, the receiver-generated pseudorandom noise codes are delayed in time with respect to directly received, line-of-sight signals. This isolates power originating from annulus zones surrounding the specular reflection point. These zones determine the spatial resolution of the GPS wind retrieval method. Let us assume a 30° incidence angle and take the largest annulus zone created by 5-chip time delay. Three satellites azimuthally separated by 120° would cover a region with about 10 km in diameter. The shape of the resulting waveform of power-versus-delay is dependent upon the roughness of the ocean surface (see Fig. 1b). This roughness is in turn a function of the surface wind speed and direction, and therefore provides a means to retrieve these geophysical parameters from the GPS-reflected signal power measurement.

3. Method for wind speed and wind direction retrieval

a. Preprocessing the data

Before the estimator can make use of the reflected GPS data, they must be preprocessed. Preprocessing takes place in several steps. First, the noise floor is computed for each dataset. This is done by computing the mean of all the points before the first correlation peak of the reflected signal. After computing the noise floor, it is subtracted from all data points. These reflected data points are then normalized by dividing by the total reflected power. Normalization is necessary to remove the effects of uncalibrated receiver gains. The total reflected power is computed by summing all of the correlation measurements for one waveform over 20 s, essentially integrating the correlation waveform. Total reflected power is chosen for normalization because it should be nearly constant due to conservation of energy. Finally, the data are broken into 1-min segments for use by the estimator.

An estimate of the path delay, τ , is computed using postprocessed positions of the satellite and receiver. The satellite positions are interpolated from International GPS Service's (IGS) 15-min precise positions, and the receiver positions are interpolated using the receiver's navigation solution. Using these positions and the GPS reference ellipsoid (also known as WGS-84, Parkinson et al. 1996a,b), an estimate of the specular reflecting point coordinates on the earth's surface is computed. The path delay is then estimated from these three positions. Because the delay variable computed from the receiver and satellite geometry with respect to the GPS reference ellipsoid may contain errors, a shifting parameter is introduced. A scaling parameter is also introduced that compensates for errors in the assumptions made during normalization of the measured power. Because the total power measured over the 10 delay bins fails

to include power over the same range of delay as the modeled waveform, inclusion of a scale factor accounts for this discrepancy during normalization. During preprocessing, we also quality-check the data and eliminate outliers by computing the mean and standard deviation of the reflected power in each delay bin.

b. Main processor

The state for the estimation process contains wind speed, wind direction, and as an option, path delay error estimates; scaling parameters can also be simultaneously estimated. For routine data processing, the software is able to estimate path delay errors by aligning the waveform leading edges.

The basis for wind direction determination is that the PDF of surface slopes is wider in the direction of the wind. This produces an asymmetry in the glistening zone. With delay measurements from a single satellite, it is not possible to unambiguously identify this asymmetry direction because the integration over a delay bin or annulus tends to obscure the uneven distribution, creating an ambiguity with respect to the asymmetry direction. Recovery is possible with multiple satellites when the glistening zones are due to the same surface wind conditions. Because the annuli for the two or more satellites are not mutually concentric, these measurements provide the necessary conditions for observing the PDF asymmetry.

In the latest version of our algorithm, we implemented the option of processing any number of satellites in a single batch to fit the measured to the modeled waveforms using a nonlinear least squares algorithm in MATLAB. In the algorithm, residuals are minimized using a Nelder–Mead simplex (direct search) method to adjust the state (see, e.g., Press et al. 1986).

By processing two or three satellites simultaneously, both wind speed and direction can be solved. To make the multiple satellite estimator code run faster, we created an extensive waveform database using combinations of receiver height, elevation angle, wind speeds, and wind directions.

4. Flights

The National Oceanic and Atmospheric Administration (NOAA) Hurricane Research Division, with the assistance of the NOAA/Environmental Technology Laboratory (ETL), installed a DMR GPS receiver in one of the WP-3D Hurricane Hunters N42RF *Kermit*. Members of the NOAA Airborne Operations Center at MacDill Air Force Base, Florida, installed the receiver in August 2000. The first data were collected during the prestorm flight to Hurricane Keith on 1 October 2000. The emergence of Hurricane Michael presented the first opportunity to traverse the core of a tropical cyclone on 18 October. Hurricane Michael formed in the western Atlantic Ocean on the evening of 16 October. It reached

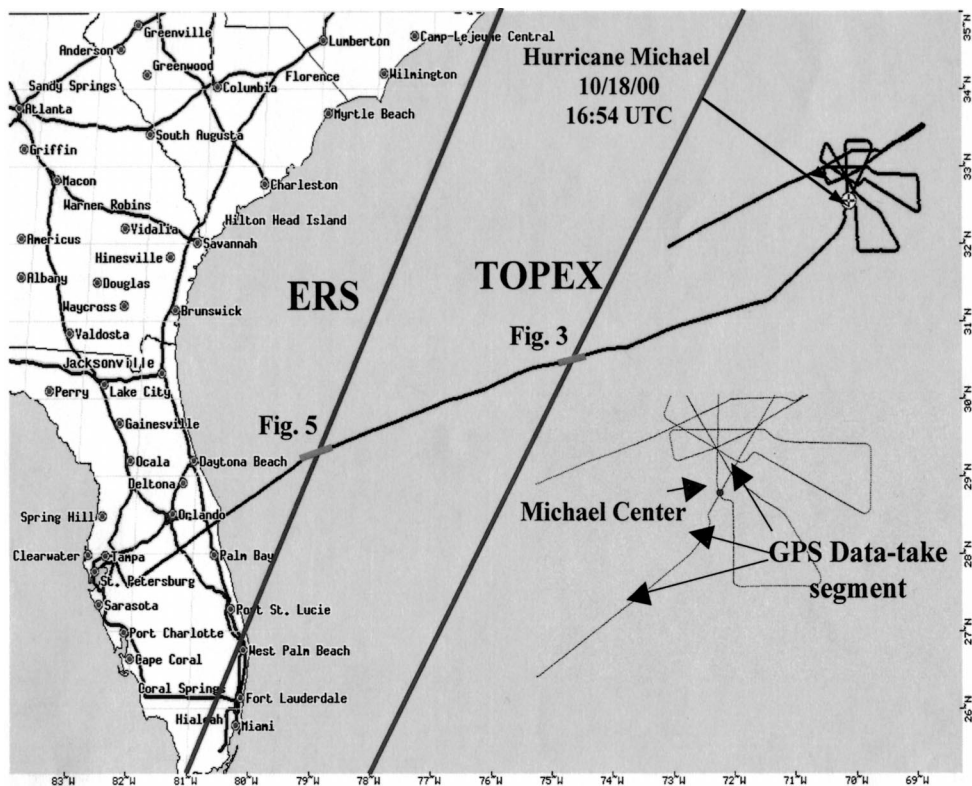


FIG. 2. Flight trajectory for Hurricane Michael of 18 Oct 2000 adapted from Katzberg et al. (2001).

tropical storm strength the next morning and was classified as a hurricane that same afternoon. Michael increased forward speed the night of 18 October. It sped northward; made landfall in Newfoundland, Canada, on 19 October; and quickly began losing tropical characteristics. At the time of the aircraft penetration, the storm was moving at approximately 18 m s^{-1} . Figure 2 is a map derived from the GPS position information, which shows the aircraft flight path from MacDill, Florida, into the center of Hurricane Michael and subsequent flying in and around storm. The cross represents the center of the storm (from Hurricane Research Division data) during the time the GPS surface reflection data were taken. Preliminary results and findings of the data processing were presented in Katzberg et al. (2001). For comparison purposes, we used wind speeds from TOPEX/Poseidon dual-frequency altimeter (Witter and Chelton 1991; TOPEX 1990), European Remote Sensing Satellites (ERS) altimeter, buoy measurements, flight-level wind speed, and onboard simultaneous-frequency microwave radiometer (SFMR2) data (see, e.g., Carswell et al. 2000; Knapp et al. 2000). The corresponding TOPEX and ERS ground trajectories are indicated in Fig. 2. In Figs. 3 and 5, the portions of the GPS flight tracks used for wind retrievals are marked with red squares. Those measurements were separated not only spatially but also in time. The time difference between ERS, TOPEX, and GPS observations was about an hour.

Also to compare GPS-derived wind vectors (speed and direction) (obtained during 1 October flight to Hurricane Keith) with an independent remote sensing measurement, we used QuikSCAT-derived wind vectors. For a detailed discussion of different satellite wind speed retrieval techniques, see Stewart (1985).

5. Results

In this section we present the results obtained during two flights of opportunity. Data obtained during the 1 October flight are used to demonstrate the ability of the GPS reflection technique for wind direction retrieval since the overflight of the QuikSCAT satellite that provided wind vector reference was close in time to the aircraft flight. For the 18 October flight we did not have a similar opportunity. Therefore, data from the 18 October flight were used only for wind speed retrieval.

a. Wind speed retrieval

During the 18 October flight to Hurricane Michael the aircraft flew out from the coast of Florida at an altitude of 4500 m. It descended to 1400 m, traversed the eye of the storm, and then descended farther to 500 m, where it remained for most of the time the GPS equipment was operated. At approximately 1550 UTC, the aircraft flight path crossed a TOPEX ground track.

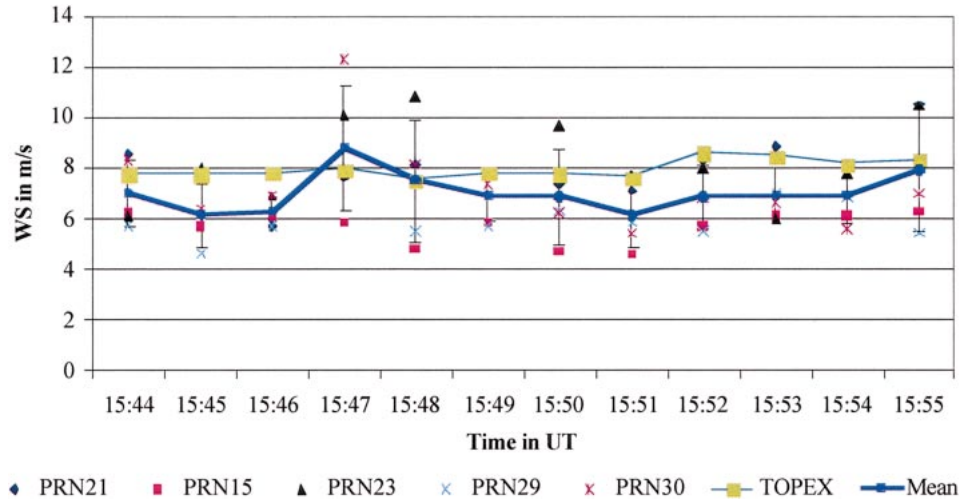


FIG. 3. Satellite-by-satellite GPS wind speed solution for TOPEX pass.

Figure 3 shows the GPS-derived wind estimates at this time based on reflected signals from satellites with pseudorandom noises (PRNs) 15, 21, 23, 29, and 30, for each satellite separately. In Fig. 3, we also plotted the mean of the individual solutions along with the standard deviations. The estimated wind speed estimates using single satellites ranges between 6 and 10 m s⁻¹. A combined solution using PRNs 15, 21, and 23 only is presented in Fig. 4. PRNs 29 and 30 were eliminated due to the relatively low elevation angles of the satellites: 32° and 41°, respectively. The combined solution in Fig. 4 agrees with the TOPEX solution within an rms of 0.7 m s⁻¹. The rms of the individual satellite estimates is 1.2 m s⁻¹.

Combining several satellites in a least squares batch solution assumes that all the glistening zones are close enough to be affected by the same wind. This means that the wind speed estimates should be valid for all

satellites in question. Including satellites with low elevation angles in the solution challenges this assumption. Using three satellites at higher elevation angles provides us with a large enough degree of freedom and computationally the system of normal equations is still manageable. Including all satellites in the combined solution does not provide us with an added advantage other than the task of having to invert a large system of normal equations.

At approximately 1455 UTC, the aircraft crossed the ERS ground track. We again processed the satellites separately, as shown in Fig. 5, along with the mean and standard deviation. A combined solution was obtained showing better agreement with the corresponding ERS measurements (0.7 m s⁻¹ rms, see Fig. 6) than the average solution from individual satellites (0.9 m s⁻¹ rms). We believe that the larger differences near the start of the graph are the result of a larger separation between

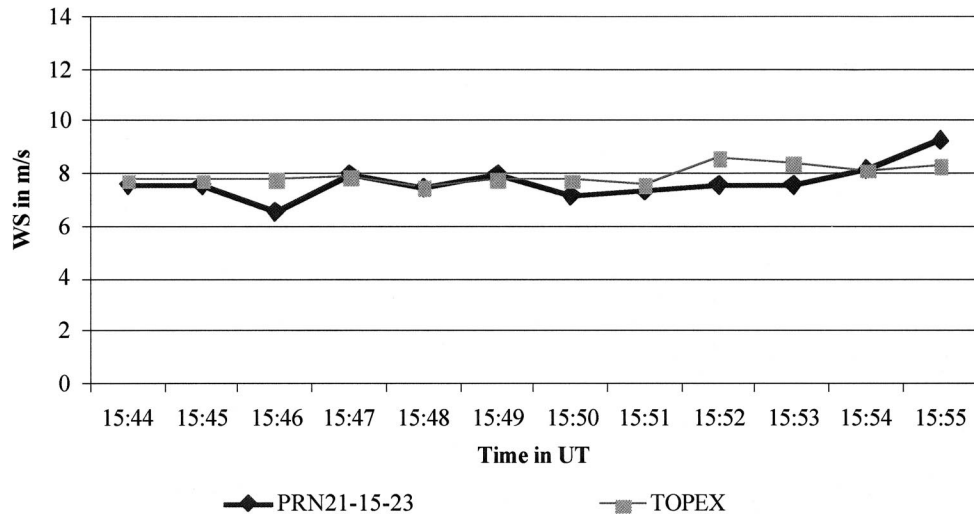


FIG. 4. Multiple-satellite GPS wind speed solution for TOPEX pass.

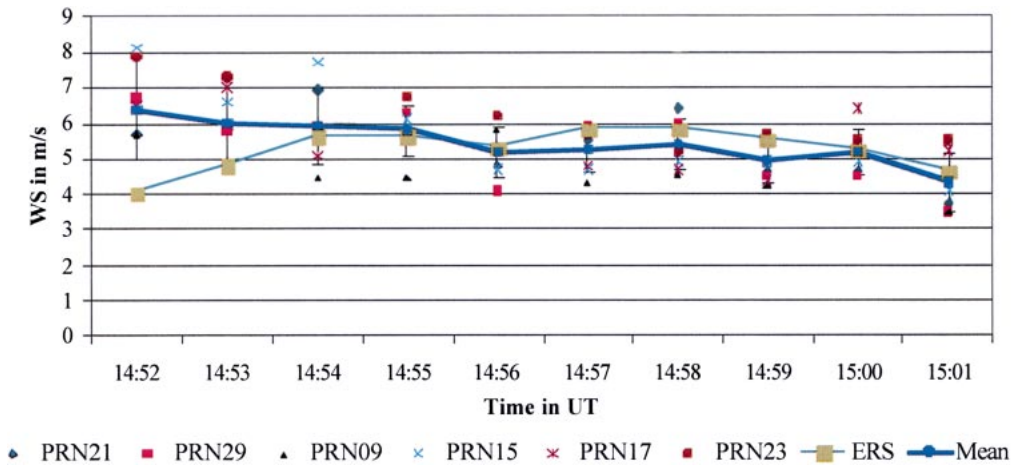


FIG. 5. Satellite-by-satellite GPS wind speed solution for ERS pass.

the aircraft position and the ERS ground track at that point.

In Fig. 7, we show the combined solution for a 3-h segment of the flight track that also included the TOPEX and ERS data segments. Also displayed is the aircraft altitude. Time tags corresponding to TOPEX and ERS passes, and buoy measurements (interpolated to the time of aircraft overflight), are superimposed and show generally good agreement between GPS wind estimates and other measurements for the prehurricane part of the flight. The separation distance between the buoy and aircraft closest approach is about 5 km.

Furthermore, data from the Hurricane Research Division of NOAA representing flight-level wind speed (FLWS) were obtained and plotted in Fig. 7. FLWS data were provided in 1-min- and 10-s-averaged time series. In Fig. 7, we plotted the 1-min-averaged datasets. FLWS data are derived from the difference of the aircraft velocity with respect to air and to the ground with recalculating it to 10-m level. It should be noted that FLWS

data gives us a rough estimate for the real 10-m-level wind speed. Therefore, we had to rely on it since it was the only reliable source of ocean-surface wind speed along the flight track. Also displayed is the time series of retrieved wind speeds from a simultaneous-frequency microwave radiometer SFMR. Rain rates are also available from the SFMR, though no rain has been reported from the SFMR data during the flight. More importantly, SFMR provided reliable wind speed measurements, even in the presence of precipitation. SFMR wind speeds have been validated using GPS dropsondes by Uhlhorn and Black (2003).

Let us first compare GPS, SFMR, and FLWS wind speed data for the prehurricane portion of the flight between 1442 and 1620 UTC that was completed at about 4.5-km altitude. Even though we have good fits with buoy, ERS, and TOPEX altimeter winds, the GPS winds exhibit systematically lower values than FLWS. This is seen in scatterplots in Fig. 8. The plot in Fig. 8a shows the SFMR wind retrievals as a function of the FLWS

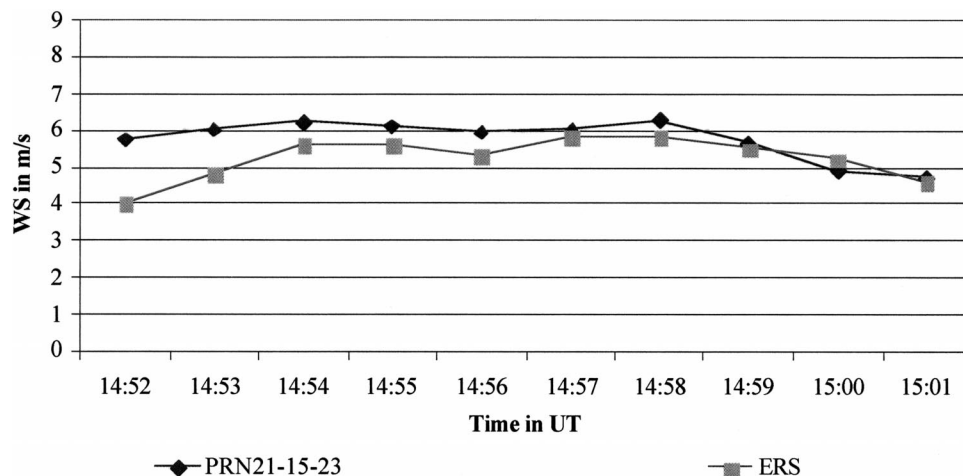


FIG. 6. Multiple-satellite GPS wind speed solution for ERS pass.

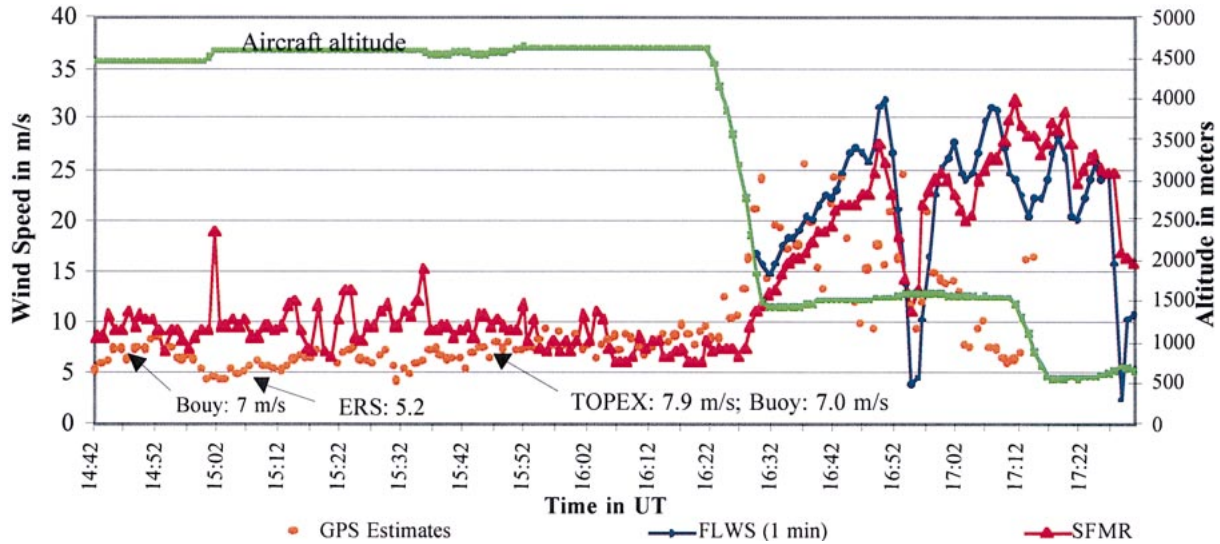


FIG. 7. GPS wind speed estimates along the flight path for Hurricane Michael on 18 Oct 2000.

wind speed. Empty circles, which correspond to the pre-hurricane portion of the flight, are grouping symmetrically around the bisector with a noticeable scatter. The corresponding GPS winds in Fig. 8b show less scatter against FLWS data, however, with a significant negative bias, which mostly originates from two flight periods: one is around 1500–1520 UTC and another one is around 1600–1620 UTC. Interestingly, the SFMR winds are closer to the GPS winds during the latter period, when the airplane approached the hurricane and FLWS started to grow (see Fig. 7).

At 1622–1630 UTC, the aircraft was descending from 4.5 to 1.5 km and entering the hurricane region. This is apparent from significant increases in the wind speed from FLWS data. The SFMR data also show an increase of wind speed but with a significant delay in time. The

GPS retrieved wind speed data demonstrate significant variations in magnitude and reveal a discrepancy with both SFMR and flight-level wind. A possible explanation for these events could be as follows. To get a correct retrieval of wind speed (and direction) we need to have a very accurate determination of the receiver altitude with respect to the reference ellipsoid. Otherwise, individual waveforms could not be properly aligned along the time delay axis, and therefore will be summed up with some spread. Ultimately, this would lead to the widening of the average waveform. Since the effects of wind also exhibit themselves through the widening of the average waveform, inaccuracy in the altitude determination produces a positive bias in wind speed retrieval. Altitude errors are more frequent during any unsteady motion of the airplane such as ascends, descends, turns,

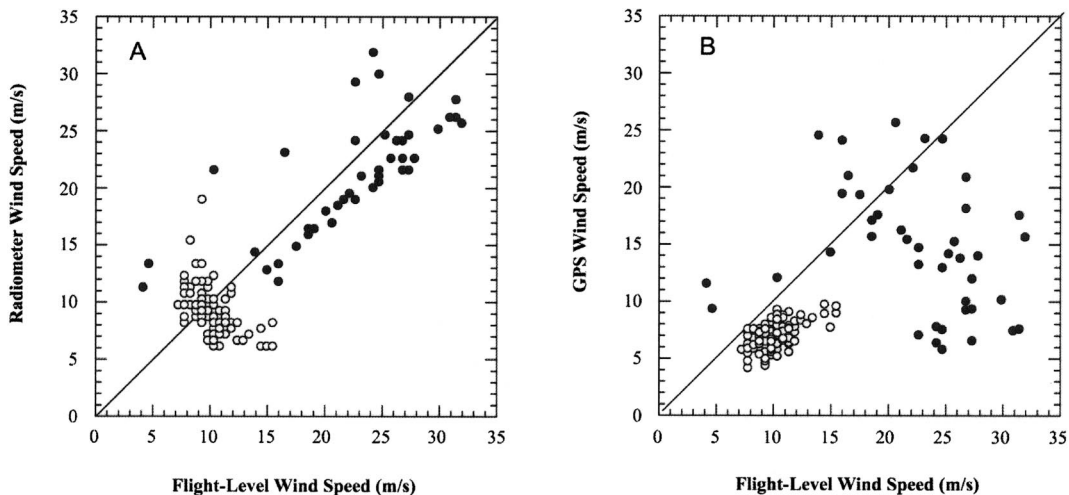


FIG. 8. Wind speed retrievals for (a) SFMR and (b) DMR as a function of the flight-level wind speed obtained along the flight path for Hurricane Michael on 18 Oct 2000.

etc., mainly for two reasons. First, it takes some time to obtain a navigation solution even for the regular GPS receiver. Therefore, when the airplane is moving unsteadily, its position is determined with some error. Second, it is known that the actual gain pattern (for both zenith and nadir antennas) is affected by multipath effects from the fuselage, wings, tail, propellers, etc. When the airplane keeps a stable altitude those signal variations are slow, so the receiver follows them without problems. During fast maneuvers those variations are also fast and behave like an additional noise. This leads to an additional error in determining the position of the airplane and therefore prevents us from a proper alignment of GPS reflected waveforms. We were aware of this problem from previous flights and from other researchers who were performing similar experiments; however, to our knowledge this problem has not been addressed in other publications.

The data obtained after descending, from 1630 to 1713 UTC, are presented in Fig. 8 by filled circles. The GPS winds in the hurricane region demonstrate a significant scatter mainly due to an inadequacy of our rough-surface spectral model to hurricane conditions. Both the time series in Fig. 7 and the scatterplot in Fig. 8b show GPS wind peak values of 25 m s^{-1} ; however, they are out of sync with FLWS data. Our spectral model taken from Elfouhaily et al. (1997) pertains to steady wind conditions with one wind direction dominating over a sufficiently large ocean area called fetch. Due to a vorticity and nonstationarity of the short-fetched wind fields within the moving hurricane, conditions of the air–sea interaction are constantly changing, which creates several systems of surface gravity waves moving in different directions (Wright et al. 2001). This rather small-scale variability of the wind (and, therefore, surface wave) field in the interior of the hurricane makes it difficult for the GPS reflection technique to follow all these spatial variations. The FLWS data are related to the winds straight below the aircraft, and, similarly, the SFMR looks at nadir. At the same time, the GPS winds originated from various glistening zones seen at different azimuthal angles and were separated by several kilometers. This also could contribute to spatial decorrelation between GPS winds and winds measured using other means.

Wind retrieval from GPS reflections usually overestimates real winds below 5 m s^{-1} (Garrison et al. 2002), probably due to comparable contribution to surface roughness from omnipresent swell. However, in our experiments, winds were above 5 m s^{-1} , and we were concerned about the ability of this technique to retrieve winds above $10\text{--}15 \text{ m s}^{-1}$. Indeed, as it follows from the analysis presented in Garrison et al. (2002) the separation between two waveforms, corresponding to two given wind speeds, becomes smaller for increasing wind speed. Therefore, for a given signal noise level the error bars are larger for higher wind speeds. More averaging would require reducing the noise; however, it would

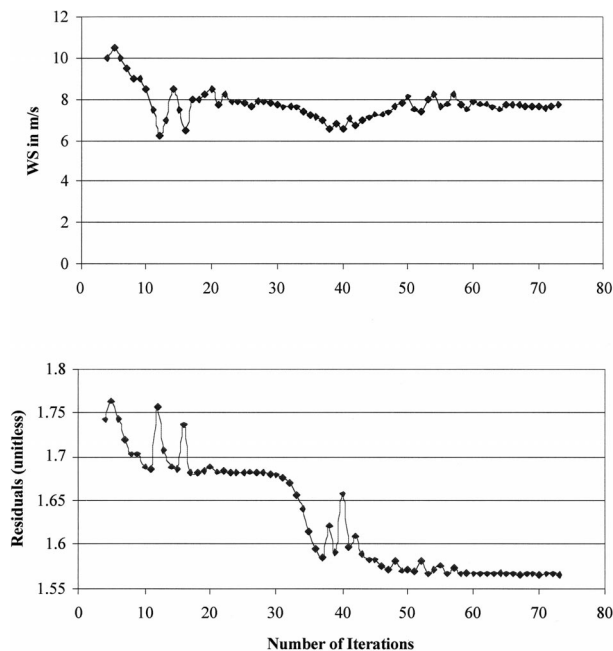


FIG. 9. An example of wind speed convergence showing dependence between number of iterations, estimated wind speed, and residuals for the TOPEX pass. Empty circles correspond to the pre-hurricane leg of the flight, and filled circles correspond to the hurricane leg.

inevitably lead to a worse spatial resolution for wind retrieval.

At around 1655 UTC, the aircraft flew over the eye of the hurricane. With all the complications mentioned above associated with GPS wind retrievals in hurricanes, the GPS wind data demonstrate a definite dip at exactly that time. The GPS technique gives there higher, about 12 m s^{-1} wind speeds, compared to 5 m s^{-1} from the FLWS data. This discrepancy is quite expected, since the eye zone is affected by swell-like waves from surrounding areas, which would give rise to GPS-retrieved winds. Notice that the SFMR also gives higher winds in the eye.

In Fig. 9, we show an example for 1544 UTC (see Figs. 3 and 4) of the estimator convergence in terms of both the wind speed estimate and the sum of the squared measurement residuals. The filter was initialized with a wind speed of 10 m s^{-1} and a scaling parameter set to unity. It is shown that after approximately 70 iterations the wind speed converges to 7.8 m s^{-1} . In most cases convergence is reached in fewer than 30 iterations when the wind speed and direction estimates are initialized with the solutions from the previous segment.

b. Wind direction retrieval

The second dataset we present is for 1 October 2000 and is taken from the area of the Gulf of Mexico, 100–200 km to the west of Florida, about 1000 miles from Hurricane Keith. The GPS reflection data have been

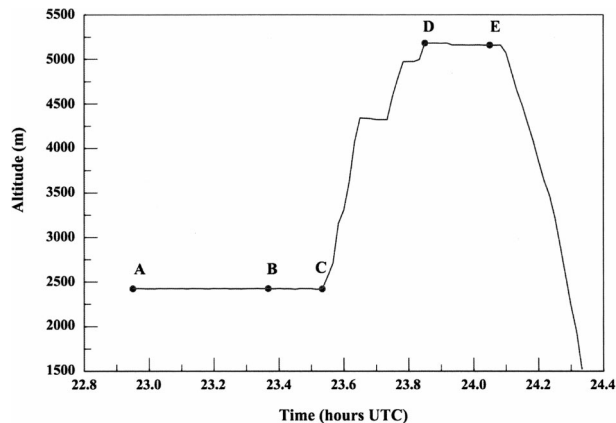


FIG. 10. Aircraft altitude at the end of the flight for Hurricane Keith on 1 Oct 2000.

obtained during the last hour of the flight to Hurricane Keith. The aircraft altitude during this portion of the flight is shown in Fig. 10. Wind speeds ranged from 6 to 10 $m s^{-1}$. What distinguishes this dataset from the Hurricane Michael dataset is that we have QuikSCAT wind field data available that was taken within 1 h of the GPS measurements. In this case, we retrieved wind speed as well as wind direction information using the multiple satellite solution from PRNs 01, 03, and 13, as described earlier.

In Fig. 11, we plot the GPS-derived wind speed and direction solution superimposed on the QuikSCAT wind field plot. The aircraft was flying from west to east. Wind speeds are plotted next to the base of the arrows representing the GPS-estimated wind directions. The sections AB and DE of the flight track show good agreement in both wind speeds and wind directions. There is a significant disagreement between GPS-estimated and QuikSCAT wind directions for the BD section of the flight track. We analyzed available data from NOAA Atlantic Oceanographic and Meteorological Laboratory (AOML) Hurricane Research Division and National Weather Service and concluded that the QuikSCAT observations for that section the flight track look more reasonable than ours. The main difference between various sections of the flight track as it is seen from Figs. 10 and 11 is the varying direction and altitude of the airplane for section BD, and the stable direction and altitude of the airplane for sections AB and DE. It seems that similar to what we had seen for the flight to the Hurricane Michael, the stability of the airplane altitude and attitude produces a significant influence on the performance of the wind direction retrieval algorithm. It turns out that these factors play an even more important role for the wind direction retrieval than that for the wind speed retrieval. This most likely occurs due to the algorithm relying on rather subtle differences in waveforms caused by the differences in wind directions.

The first few GPS wind direction estimates near point A show some fluctuations even though the wind speeds

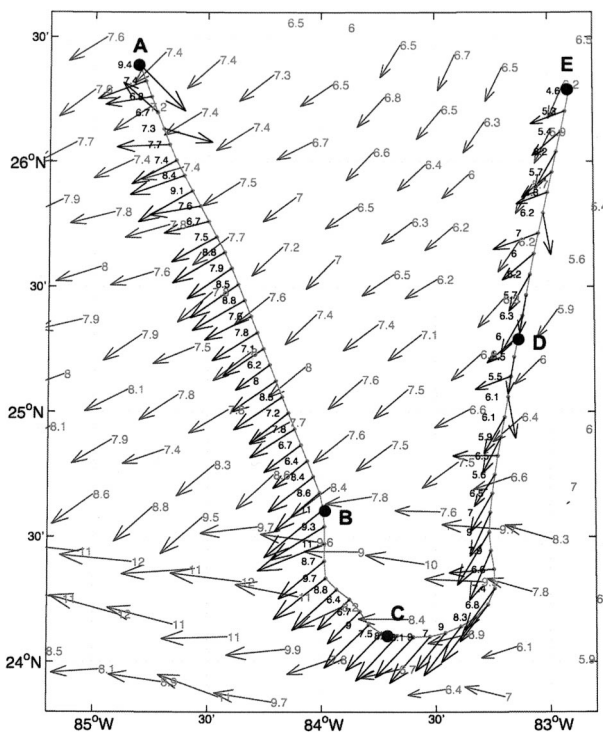


FIG. 11. GPS-derived wind vector estimates at the end of the flight for Hurricane Keith on 1 Oct 2000 overlaid on QuikSCAT wind field measurements.

are consistent with QuikSCAT data, and the airplane is at a stable geometry. The discrepancy in wind direction might be due to the fact that our estimator flagged too many data points as outliers, resulting in a smaller number of waveforms being available to the estimator.

In Fig. 12, we plotted an example for estimated wind speed, wind direction, and residuals to demonstrate the convergence of the solution on the accepted truth. It is shown that after 40 iterations the solution converges on 7.6 $m s^{-1}$ wind speed and about 30° wind direction. QuikSCAT indicates 7.6–7.8 $m s^{-1}$ wind speed and about 40° wind direction.

6. Error analysis

In this section, we investigate the nonlinear wind speed and wind direction estimator convergence properties. In Figs. 13 and 14, we computed the combined solution residuals using all possible combinations of wind speed (1 $m s^{-1}$ increments) and wind directions (10° increments). In Fig. 13, it is shown that the minimum of the residuals occurs for wind speeds between 6 and 8 $m s^{-1}$. On the other hand, in Fig. 14, we show that the minimum of the residuals are obtained for wind direction between 20° and 40°. The individual curves represent a solution with different wind speeds between 4 and 10 $m s^{-1}$ starting with 4 $m s^{-1}$ at the top. We can clearly see that the difference between measured and

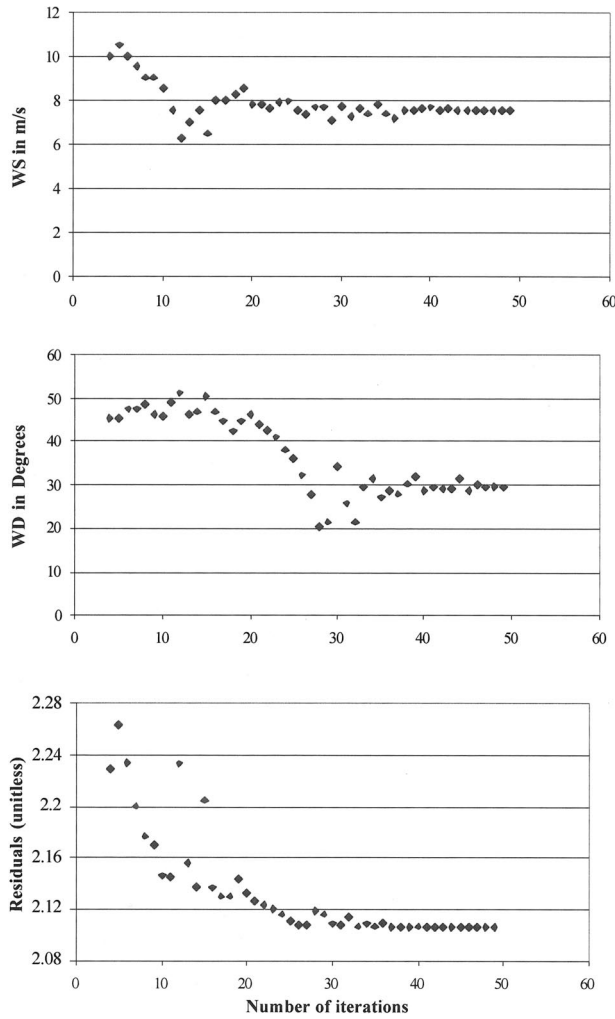


FIG. 12. An example for wind speed and wind direction convergence for 1 Oct 2000.

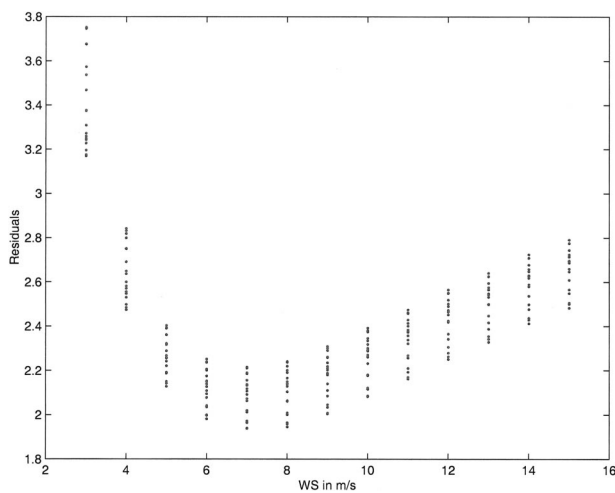


FIG. 13. Residuals (unitless) vs wind speed for 1 Oct dataset.

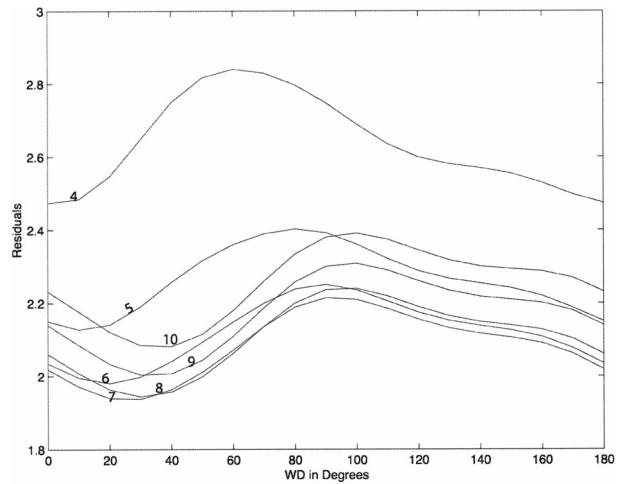


FIG. 14. Residuals (unitless) vs wind direction for 1 Oct dataset.

modeled values (the residuals) is at the minimum when the right answer (WS and WD) is used to compute the measurement residuals. Figure 14 points out that in the vicinity of the QuikSCAT results (7 or 8 m s⁻¹) there are solutions with combinations of wind speeds and wind directions resulting in the same sum of the squared residuals. To demonstrate this, we plotted the residuals using combinations of wind speeds and wind directions. In Fig. 15, isoresidual lines show possible combinations of wind speeds and wind directions resulting in the same minimum of the sum of the squared residuals. The “hole” in the middle shows a set of solutions close to the final solution. However, the estimator indicates that the sum of the squared residuals is at the minimum at the middle of the “hole” that can be characterized with wind speed of 7.6 m s⁻¹ and wind direction of 30°, which is in very good agreement with the QuikSCAT measurements.

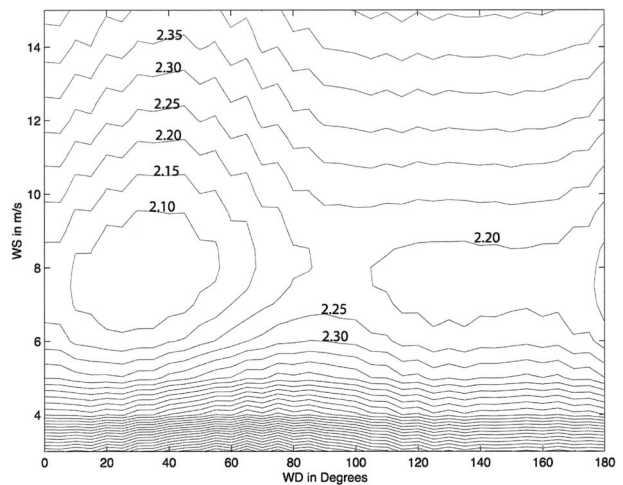


FIG. 15. Wind direction, wind speed, and residuals map for the combined multisatellite solution.

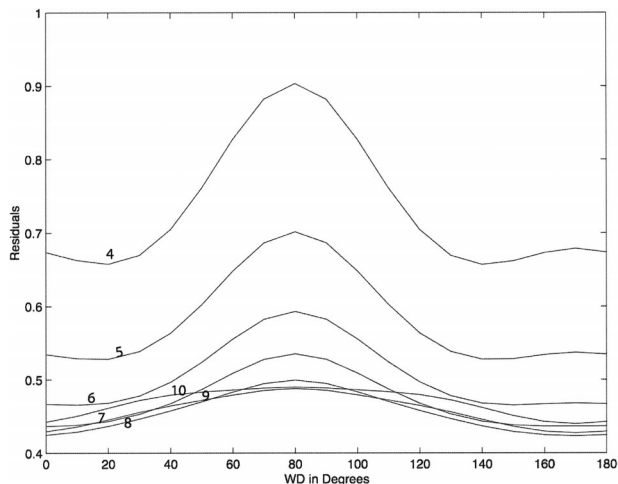


FIG. 16. Illustration of unreliable wind direction estimation using a single satellite (PRN30).

A reliable wind direction estimate cannot be obtained using delay measurements from a single satellite. This is demonstrated in Fig. 16. Although the estimated wind speed is about 8 m s^{-1} , the wind direction is estimated to be near 140° , coinciding with the incidence angle of the satellite with an additional ambiguity at about 20° . There are two types of ambiguities in the GPS wind direction retrieval. First, there is a 180° ambiguity that is related to the symmetry of the PDF of slope in up/down wind direction. This ambiguity cannot be resolved even using multiple satellites. Second, there is the ambiguity related to the symmetry with respect to the incidence plane. Indeed, there are two possible angles between the incidence plane and wind direction that create the same GPS-reflected signal power. Therefore, the ambiguity can only be solved for using additional simultaneously observed satellites. In Fig. 17, we plotted the map of wind speeds and wind directions using one satellite only. The estimator shows a larger pool of possible solutions before finally arriving at 8 m s^{-1} wind speed and 170° wind direction (aligned with the incident plane).

We also computed the repeatability of the solutions based upon consecutive and independent 1-min data segments with the same three satellites. We assume that the wind speed and wind direction do not change over a 10-min window. Computing the repeatability gives a measure of the effect of measurement noise on the actual solution. This analysis shows that over a 10-min arc, the standard deviations of the wind speed and direction are 0.7 m s^{-1} and 9° , respectively. As to the accuracy of our GPS-derived wind direction estimates, the processed data using the combined solution indicated a better than 30° agreement with the QuikSCAT measurement for stable flight conditions. This is encouraging since the overall reported QuikSCAT wind direction accuracy is about 20° (see e.g., QuikSCAT 2002).

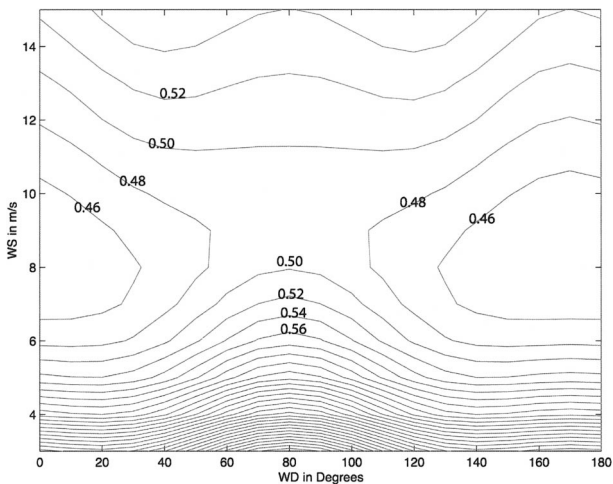


FIG. 17. Wind direction, wind speed, and residuals map using a single satellite (PRN30).

7. Conclusions and future research

We have demonstrated wind speed and wind direction retrievals using a novel multisatellite approach combined with nonlinear least squares estimation. GPS-derived wind speed and wind direction is compared with TOPEX, ERS, buoy, and QuikSCAT measurements. We found that processing surface-reflected GPS signals in a combined solution, as opposed to a satellite-by-satellite solution, gives us better wind speed agreement, at the level of 2 m s^{-1} on an average, with other independent techniques for wind speeds between 5 and 10 m s^{-1} . A comparison between GPS-derived wind direction and a portion of QuikSCAT wind field showed a better than 30° agreement in wind direction. We also demonstrated that it is not possible to estimate wind direction with delay measurements from a single satellite.

At the same time, some retrieved data exhibit biases and significant variations and departures from those obtained with other means. The analysis of data shows that at moderate winds most discrepancies occur when the airplane is changing either the altitude or direction, or both. During the unsteady flight, an additional source of error is originated from an inaccurate determination of the receiver altitude. These altitude errors do not allow a satisfactory alignment of individual waveforms during the process of incoherent averaging of the signal. Ultimately, this leads to a widening of the average waveform resulting in a positive bias in wind speed retrieval. The unsteady motion of the airplane is even more detrimental for the wind direction retrievals. More work is needed on postprocessing algorithms that will either filter out the affected data or compensate for those geometrical changes.

It is relevant to mention another possible source of discrepancies associated with high wind speed conditions. The current instrument with a relatively low sig-

nal-to-noise ratio/data rate and the ocean surface model using an assumption of well-developed stationary seas are not well suited for the strong wind speed determination. More GPS reflection measurements with improved DMR receivers, an enhanced surface model that accounts for more variable conditions, better independent/in situ observations, and improvements to data quality and processing are required to achieve progress in these more challenging conditions.

Acknowledgments. This research has been sponsored at the University of Colorado by a grant from NASA HQ (NAG5-9727), and at NOAA/ETL by RTOP 622-47-55. We appreciated the assistance of Dr. Peter Black and Steve Feuer of the NOAA/AOML Hurricane Research Division in providing us with the wind speed data. We would like to thank the anonymous reviewers for very useful critical comments and suggestions.

REFERENCES

- Armatys, M., D. Masters, A. Komjathy, P. Axelrad, and J. L. Garrison, 2000: Exploiting GPS as a new oceanographic remote sensing tool. *Proc. ION National Technical Meeting*, Anaheim, CA, Institute of Navigation, CD-ROM, 339.
- Bass, F. G., and I. M. Fuks, 1979: *Wave Scattering from Statistically Rough Surfaces*. International Series in Natural Philosophy, Vol. 93, Pergamon Press, 527 pp.
- Carswell, J. R., E. J. Knapp, P. S. Chang, P. D. Black, and F. D. Marks, 2000: Limitations of scatterometry high wind speed retrieval. *Proc. IEEE Int. Geoscience and Remote Sensing Symp. (IGARSS): Taking the Pulse of the Planet: The Role of Remote Sensing in Managing the Environment*, Piscataway, NJ, IEEE, 1226–1228.
- Elfouhaily, T., B. Chapron, K. Katsaros, and D. Vandemark, 1997: A unified directional spectrum for long and short wind-driven waves. *J. Geophys. Res.*, **102**, 15 781–15 796.
- Garrison, J. L., and S. J. Katzberg, 2000: The application of reflected GPS signals to ocean remote sensing. *Remote Sens. Environ.*, **73**, 175–187.
- , —, and C. T. Howell, 1997: Detection of ocean reflected GPS signals: Theory and experiment. *Proc. IEEE Southeastcon*, Blacksburg, VA, IEEE, 290–294.
- , —, and M. I. Hill, 1998: Effect of sea roughness on bistatically scattered range coded signals from the Global Positioning System. *Geophys. Res. Lett.*, **25**, 2257–2260.
- , A. Komjathy, V. U. Zavorotny, and S. J. Katzberg, 2002: Wind speed measurement using forward scattered GPS signals. *IEEE Trans. Geosci. Remote Sens.*, **40**, 50–65.
- Katzberg, S. J., and J. L. Garrison, 1996: Utilizing GPS to determine ionospheric delay over the ocean. NASA Tech. Memo. 4750, 14 pp.
- , R. A. Walker, J. H. Roles, T. Lynch, and P. G. Black, 2001: First GPS signals reflected from the interior of a tropical storm: Preliminary results from Hurricane Michael. *Geophys. Res. Lett.*, **28**, 1981–1984.
- Knapp, E. J., J. R. Carswell, and C. T. Swift, 2000: A dual polarization multi-frequency microwave radiometer. *Proc. IEEE Int. Geoscience and Remote Sensing Symp. (IGARSS): Taking the Pulse of the Planet: The Role of Remote Sensing in Managing the Environment*, Piscataway, NJ, IEEE, 3160–3162.
- Komjathy, A., V. U. Zavorotny, and J. L. Garrison, 1999: GPS: A new tool for ocean science. *GPS World*, **10**, 50–56.
- , —, P. Axelrad, G. H. Born, and J. L. Garrison, 2000: GPS signal scattering from sea surface: Comparison between experimental data and theoretical model. *Remote Sens. Environ.*, **73**, 162–174.
- Lin, B., S. J. Katzberg, J. L. Garrison, and B. A. Wielicki, 1999: The relationship between the GPS signals reflected from sea surface and the surface winds: Modeling results and comparisons with aircraft measurements. *J. Geophys. Res.*, **104** (C9), 20 713–20 727.
- Lowe, S. T., C. Zuffada, J. L. LaBrecque, M. Lough, J. Lerma, and L. E. Young, 2000: An ocean-altimetry measurement using reflected GPS signals observed from a low-altitude aircraft. *Proc. IEEE Int. Geoscience and Remote Sensing Symp. (IGARSS): Taking the Pulse of the Planet: The Role of Remote Sensing in Managing the Environment*, Honolulu, HI, IEEE, CD-ROM, INT30.02.
- , J. L. LaBrecque, C. Zuffada, L. J. Romans, L. E. Young, and G. A. Hajj, 2002: First spaceborne observation of an earth-reflected GPS signal. *Radio Sci.*, **37**, 1–28.
- Martin-Neira, M., 1993: A passive reflectometry and interferometry system (PARIS) application to ocean altimetry. *ESA J.*, **17**, 331–355.
- , M. Capparini, J. Font-Rossello, S. Lannelongue, and C. S. Vallmitjana, 2001: The PARIS concept: An experimental demonstration of sea surface altimetry using GPS reflected signals. *IEEE Trans. Geosci. Remote Sens.*, **39**, 142–150.
- Parkinson, B. W., J. J. Spilker, P. Axelrad, and P. Enge, Eds., 1996a: *Global Positioning System: Theory and Applications*. Vol. 1. American Institute of Aeronautics and Astronautics, 794 pp.
- , —, —, and —, Eds., 1996b: *Global Positioning System: Theory and Applications*. Vol. 2. American Institute of Aeronautics and Astronautics, 645 pp.
- Press, W. H., B. P. Flannery, S. A. Teukolsky, and W. T. Vetterling, 1986: *Numerical Recipes: The Art of Scientific Computing*. Cambridge University Press, 818 pp.
- QuikSCAT, cited 2002: Quikscat: Satellite fact sheet. [Available online at <http://www.tbs-satellite.com/tse/online/sat-quickscat.html>.]
- Stewart, R. H., 1985: *Methods of Satellite Oceanography*. University of California Press, 360 pp.
- TOPEX, 1990: TOPEX ground system science algorithm specification. Jet Propulsion Laboratory Publ. JPL 633-708, D-7075, 352 pp.
- Treuhaft, R. N., S. T. Lowe, C. Zuffada, and Y. Chao, 2001: Two-cm GPS altimetry over Crater Lake. *Geophys. Res. Lett.*, **28**, 4343–4346.
- Uhlhorn, E. W., and P. G. Black, 2003: Verification of remotely sensed sea surface winds in hurricanes. *J. Atmos. Oceanic Technol.*, **20**, 99–116.
- Valenzuela, G. R., 1978: Theories for the interaction of electromagnetic and oceanic waves—A review. *Bound.-Layer Meteor.*, **13**, 61–85.
- Witter, D. L., and D. B. Chelton, 1991: A Geosat altimeter wind speed algorithm and a method for altimeter wind speed algorithm development. *J. Geophys. Res.*, **96**, 8853–8860.
- Wright, C. W., and Coauthors, 2001: Hurricane directional wave spectrum spatial variation in the open ocean. *J. Phys. Oceanogr.*, **31**, 2472–2488.
- Zavorotny, V. U., and A. G. Voronovich, 2000: Scattering of GPS signals from the ocean with wind remote sensing application. *IEEE Trans. Geosci. Remote Sens.*, **38**, 951–964.